Inorganic Chemistry
ARTICLE
pubs.acs.org/IC

Alloyed $(ZnSe)_x(CuInSe_2)_{1-x}$ and $CuInSe_xS_{2-x}$ Nanocrystals with a Monophase Zinc Blende Structure over the Entire Composition Range

Shenjie Li,[†,‡] Zechen Zhao,[†,‡] Qinghui Liu,[†] Lijian Huang,[†] Gang Wang,[†] Daocheng Pan,[*,†] Hongjie Zhang,[*,†] and Xingquan He[*,‡]

[†]State Key Laboratory of Rare Earth Resource Utilization, Changchun Institute of Applied Chemistry, Chinese Academy of Sciences, Graduate School of the Chinese Academy of Sciences, 5625 Renmin Street, Changchun, P. R. China 130022

[‡]Changchun University of Science and Technology, 7089 Weixing Road, Changchun, Jilin, P. R. China 130022

S Supporting Information

ABSTRACT: Metastable zinc blende $CuInSe_2$ nanocrystals were synthesized by a hot-injection approach. It was found that the lattice mismatches between zinc blende $CuInSe_2$ and ZnSe as well as $CuInSe_2$ and $CuInS_2$ are only 2.0% and 4.6%, respectively. Thus, alloyed $(ZnSe)_x(CuInSe_2)_{1-x}$ and $CuInSe_xS_{2-x}$ nanocrystals with a zinc blende structure have been successfully synthesized over the entire composition range, and the band gaps of alloys can be tuned in the range from 2.82 to 0.96 eV and 1.43 to 0.98 eV, respectively. These alloyed $(ZnSe)_x(CuInSe_2)_{1-x}$ and $CuInSe_xS_{2-x}$ nanocrystals with a broad tunable band gap have a high potential for photovoltaic and photocatalytic applications.

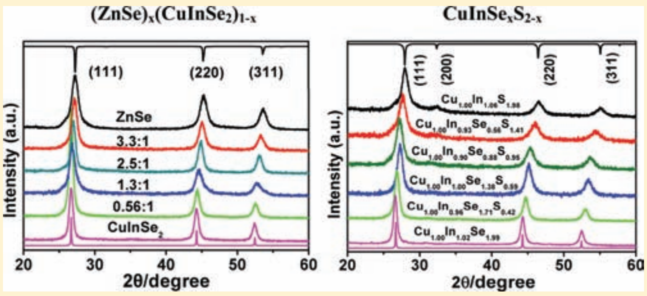

1. INTRODUCTION

Alloyed semiconductor nanocrystals with a tunable composition and band gap have received a great deal of attention as luminescent quantum dots and absorbers for thin film solar cells over the past decade, such as $Zn_xCd_{1-x}S$,[1] $Zn_xCd_{1-x}Se$,[2] $Zn_xCd_{1-x}Se_yS_{1-y}$,[3] $CdTe_xSe_{1-x}$,[4] $CuIn_xGa_{1-x}S_2$,[5] $CuIn_xTl_{2-x}S_{3.5}$,[6] $CuGa_xIn_{1-x}Se_2$,[7,8] $CuInSe_xS_{2-x}$,[9] etc. Group II−VI or I−III−VI_2 alloyed semiconductors have been extensively studied because of their potential applications in electro-optical devices[10,11] and solar cells.[12−14] They both have a high value of absorption coefficient (10^4-10^5 cm^{-1}) in the visible and near-infrared light range. To date, much of the research has focused on group II−VI or group I−III−VI_2 alloyed semiconductors. In contrast, there is little published work focused on the synthesis of alloyed $(II-VI)_x$-$(I-III-VI_2)_{1-x}$ semiconductor nanocrystals.[15−20] For alloyed $(II-VI)_x(I-III-VI_2)_{1-x}$ semiconductors, they are being considered as a replacement for the highly toxic group II−VI quantum dots[19] such as CdTe and CdSe as well as for the pure group I−III−VI_2 absorbers such as $CuIn_xGa_{1-x}Se_2$ in solar cells.[21] However, group II−VI semiconductors usually crystallize in zinc blende structure and have a space group of $F\bar{4}3m$ (216), which is totally different with group I−III−VI_2 chalcopyrite semiconductors (space group $I\bar{4}2d$, 122).[21−25] The phase separation will occur in their middle composition range.[21−25]

$CuInSe_2$ is one of the most important group I−III−VI_2 semiconductors and of particular interest in luminescent quantum dots[26,27] and solar cells.[14,28] $CuInSe_2$ has a band gap of 1.04 eV,[29] which makes it not a good choice for single-junction solar cells.[30] Therefore, alloying gallium into $CuInSe_2$ has been extensively studied, aiming to expand the band gap of $CuInSe_2$.[7,8,31−34] Currently, alloyed $CuGa_xIn_{1-x}Se_2$ thin film solar cells have demonstrated a power conversion efficiency of nearly 20%.[34] However, gallium as a rare metallic element is expensive, which is not beneficial to reduce the material cost of solar cells. In addition, the band gaps of alloyed $CuGa_xIn_{1-x}Se_2$ can be only tuned in the range from 1.7 to 1.04 eV, which cannot meet the requirements of tandem solar cells.[30] It is well known that the band gap of $(ZnSe)_x(CuInSe_2)_{1-x}$ alloys can be tuned from 2.7 to 1.04 eV, making this alloyed material uniquely suitable for optoelectronic and photovoltaic device applications.[21−24] However, it is quite difficult to synthesize homogeneous $(ZnSe)_x$-$(CuInSe_2)_{1-x}$ alloys with arbitrary composition due to their phase disparity. According to the diagram of $(ZnSe)_x(CuInSe_2)_{1-x}$, in the bulk solid solution of the $(ZnSe)_x(CuInSe_2)_{1-x}$ system,[21−25] the zinc blende structure can be only retained for up to 30 mol % of $CuInSe_2$. The phase difference between ZnSe and $CuInSe_2$ (zinc blende vs chalcopyrite) presents a significant obstacle for synthesis of homogeneous $(ZnSe)_x(CuInSe_2)_{1-x}$ alloys over the full compositional range.[21−25]

Recently, ternary $CuInS_2$ and Cu_2SnS_3 nanocrystals with a metastable zinc blende and wurtzite structure have been successfully prepared by a hot-injection approach.[17,37] Thus, alloyed $ZnS-CuInS_2-Cu_2SnS_3$ system can be synthesized with a

Received: May 22, 2011
Published: September 26, 2011

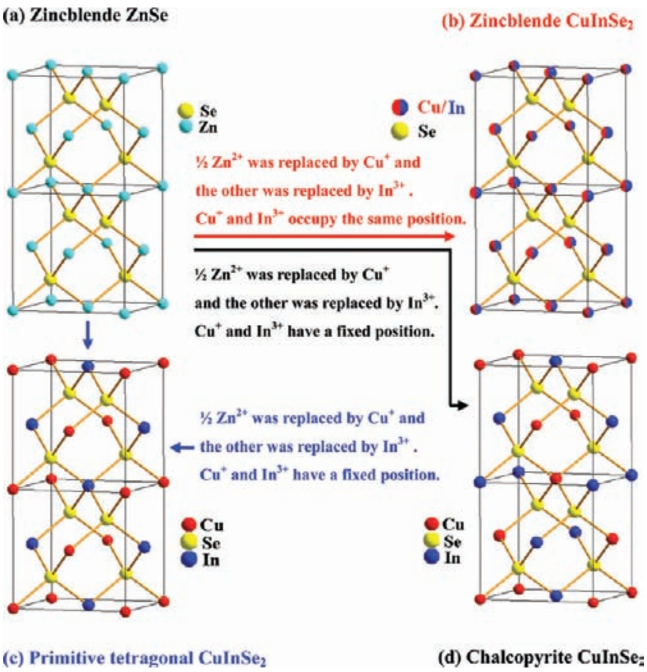

Figure 1. Double unit cells of (a) zinc blende ZnSe, (b) zinc blende $CuInSe_2$, and (c) primitive tetragonal $CuInSe_2$ as well as the unit cell of (d) chalcopyrite $CuInSe_2$.

monophase structure over the entire composition range.[15,17] Because alloyed $(ZnS)_x(CuInS_2)_y(Cu_2SnS_3)_{1-x-y}$ nanocrystals can be accessible, it is reasonable to make homogeneous alloyed $(ZnSe)_x(CuInSe_2)_y(Cu_2SnSe_3)_{1-x-y}$ nanocrystals with a monophase structure. More recently, zinc blende and wurtzite $CuInSe_2$ nanocrystals have been successfully synthesized,[28,38,39] providing a possibility to synthesize alloyed $(ZnSe)_x(CuInSe_2)_{1-x}$ nanocrystals with a structural homogeneity.

In addition, sulfur was also introduced into $CuInSe_2$ in order to expand the band gap of $CuInSe_2$ and improve the conversion efficiency of alloyed $CuInSe_xS_{2-x}$ thin film solar cells.[35,36] Recently, alloyed $CuInSe_xS_{2-x}$ nanocrystals with a chalcopyrite structure have been reported by a warm-up technique.[9] In this paper, alloyed $CuInSe_xS_{2-x}$ nanocrystals with a metastable zinc blende structure were synthesized by a hot-injection approach.

2. RESULTS AND DISCUSSION

Ternary $CuInSe_2$ can be considered as being derived from binary ZnSe. There are three main possibilities from binary ZnSe to ternary $CuInSe_2$ (see Figure 1). First, as shown in Figure 1d, Zn^{2+} can be substituted by 1/2 Cu^+ and 1/2 In^{3+} cations and Cu^+ and In^{3+} have a fixed position in the unit cell. In this case, the most common and stable chalcopyrite structure was obtained. In numerous experimental studies, $CuInSe_2$ thin film and nanocrystals usually possess a stable chalcopyrite phase.[21−28] According to the $CuInSe_2$ phase diagram, the tetragonal chalcopyrite structure is converted to a metastable zinc blende structure at temperatures higher than 810 °C,[24,25] where Cu^+ and In^{3+} cations randomly occupy the same position in the zinc blende unit cell and the occupancy possibilities of Cu^+ and In^{3+} are 50%, respectively (see Figure 1b). It is noteworthy that zinc blende ZnSe and $CuInSe_2$ possess the same space group and similar X-ray diffraction (XRD) pattern, but the zinc blende structure is metastable for ternary $CuInSe_2$ at low temperatures.

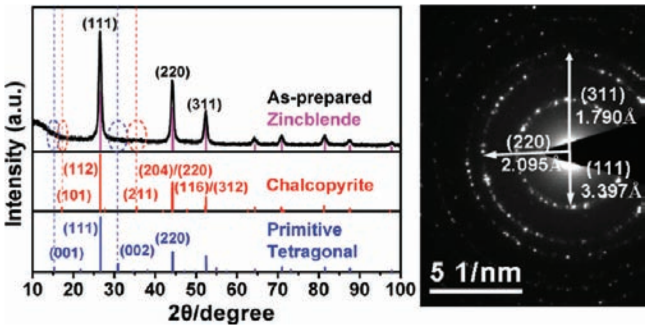

Figure 2. (Left) Comparison of experimental and simulated XRD patterns for $CuInSe_2$. (Right) Selected area electron diffraction (SAED) image of $CuInSe_2$ nanocrystals with a zinc blende structure.

Finally, another possible substitution from ZnSe to $CuInSe_2$ is shown in Figure 1c, i.e., primitive tetragonal phase. However, there are no reports on this structure in the literature.

Figure 2(left) shows the XRD pattern of as-prepared $CuInSe_2$ nanocrystals by a hot-injection technique. It is well known that the nanocrystalline structure can be different from that of the corresponding bulk materials. By changing the reactivity of precursors and/or bonding strength of capping agents, some of the high-temperature and metastable phases can be achieved for nanocrystalline materials by wet chemical methods at low temperatures. To clarify the crystalline structure of $CuInSe_2$ nanocrystals, we therefore simulated the XRD patterns for zinc blende, chalcopyrite, and primitive tetragonal $CuInSe_2$ and compared them with our experimental pattern. The simulated XRD patterns were obtained according to the unit cells in Figure 1b, 1c, and 1d using a Diamond 3.0 program, and the peaks with intensity values below 1% were ignored. It was found that our diffraction patterns did not match those of chalcopyrite and primitive tetragonal structures. The XRD pattern of as-prepared $CuInSe_2$ nanocrystals more closely resembles that of zinc blende $CuInSe_2$ rather than those of chalcopyrite and primitive tetragonal $CuInSe_2$, signifying that $CuInSe_2$ nanocrystals possess a zinc blende structure. Furthermore, the zinc blende structure of $CuInSe_2$ nanocrystals can also be confirmed by selected area electron diffraction (SAED) (Figure 2, right).

The crystallinity and crystal phase of alloyed $(ZnSe)_x(CuInSe_2)_{1-x}$ and $CuInSe_xS_{2-x}$ nanocrystals were demonstrated by the XRD shown in Figure 3 (left and right). The XRD patterns of the pure ZnSe, $CuInS_2$, and $CuInSe_2$ match their standard or simulated zinc blende patterns. All of the patterns can be indexed to a zinc blende structure, which consists of three prominent peaks consistent with the (111), (220), and (311) planes, confirming that the crystal structure of the nanocrystals is independent of the composition. Our XRD data show that even alloying a large amount of $CuInSe_2$ into ZnSe does not change the zinc blende structure of alloyed $(ZnSe)_x(CuInSe_2)_{1-x}$ nanocrystals, i.e., a monophase zinc blende structure was retained over the entire composition range. The cell parameters of alloyed $(ZnSe)_x(CuInSe_2)_{1-x}$ and $CuInSe_xS_{2-x}$ were calculated by JADE 5.0 and plotted as a function of $CuInSe_2$ mole fraction as shown in Figure 4. The calculated lattice mismatches between ZnSe and $CuInSe_2$ as well as $CuInS_2$ and $CuInSe_2$ are only 2.0% and 4.6%, and such insignificant mismatches make it possible to synthesize homogeneous $(ZnSe)_x(CuInSe_2)_{1-x}$ and $CuInSe_xS_{2-x}$ nanocrystals. As shown in Figure 4, the cell parameters of alloyed $(ZnSe)_x(CuInSe_2)_{1-x}$ and $CuInSe_xS_{2-x}$ nanocrystals were

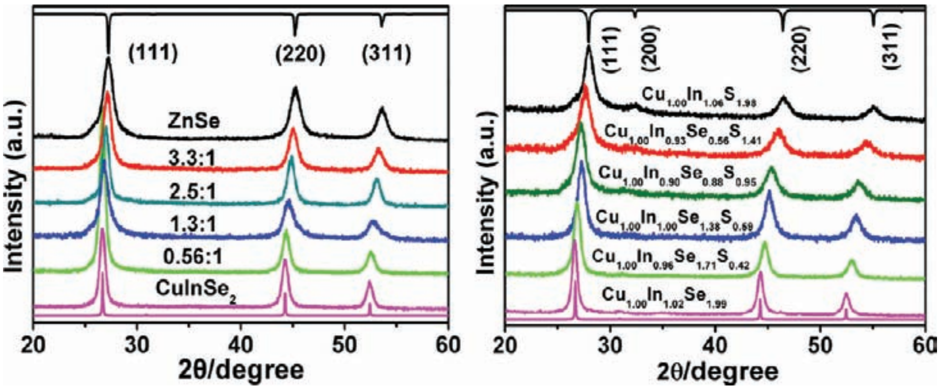

Figure 3. (Left) XRD patterns of $(ZnSe)_x(CuInSe_2)_{1-x}$ nanocrystals with a zinc blende structure. Top and bottom lines are the standard XRD pattern (PDF No. 37-1463) for zinc blende ZnSe and simulated XRD pattern for zinc blende $CuInSe_2$. (Right) XRD patterns of $CuInSe_xS_{2-x}$ nanocrystals with a zinc blende structure. Top and bottom lines are the simulated XRD patterns for zinc blende $CuInS_2$ and $CuInSe_2$.

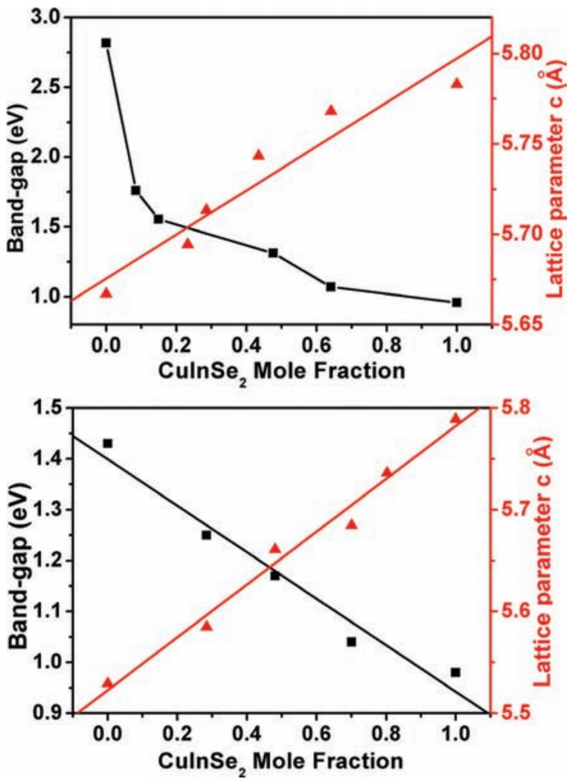

Figure 4. Lattice parameters *c* and optical band gaps of $(ZnSe)_x$-$(CuInSe_2)_{1-x}$ (top) and $CuInSe_xS_{2-x}$ (bottom) nanocrystals as a function of $CuInSe_2$ mole fraction.

increasing linearly with increasing the amount of $CuInSe_2$, which is in accordance with Vegard's law, confirming formation of homogeneous alloyed nanocrystals. Note that the reaction temperature plays a critical role in the synthesis of homogeneous $(ZnSe)_x(CuInSe_2)_{1-x}$ nanocrystals. If the temperature is below 280 °C, phase separation will occur, resulting from the low reactivity of Zn precursor. In addition, in our experiments, cation precursors were injected into a hot selenium and/or sulfur solution due to a low decomposition temperature of Cu precursor.

Although binary ZnSe and ternary $CuInSe_2$ have the same crystal structure, the band gap of the former compound was substantially larger than that of the latter. Hence, the band gap of alloyed $(ZnSe)_x(CuInSe_2)_{1-x}$ should be tuned between their band gaps. As shown in Figure 5 on the left, the optical absorption band edges of alloyed nanocrystals showed a gradual red shift with decreasing $ZnSe/CuInSe_2$ ratio. As expected, the band gap of $(ZnSe)_x(CuInSe_2)_{1-x}$ nanocrystals is continuously adjustable from 2.82 eV for pure ZnSe to 0.96 eV for pure $CuInSe_2$, which covers the optimal band gap of 1.3 eV for a single-junction solar cell.[30] For zinc blende $CuInSe_2$ nanocrystals, the band gap is slightly lower than that already reported for chalcopyrite $CuInSe_2$ (1.02−1.19 eV),[14,28,29,38,39] which is probably due to the phase disparity.

The band gap control is critically important for solar cell semiconductors and luminescent quantum dots. Therefore, the relation between the alloy compositions and their band gaps was investigated. In general, the band gaps of the alloy nanocrystals $E_g(x)$ vs compositions can be expressed as $E_g(x) = xE_g^{CuInSe_2} + (1 - x)E_g^{ZnSe} - bx(1 - x)$, where $E_g^{CuInSe_2}$ and E_g^{ZnSe} are the band gap of $CuInSe_2$ and ZnSe, respectively, x is mole fraction of $CuInSe_2$, and b is the band gap bowing parameter that characterizes the deviation from a linear relation between the band gap and the composition. Figure 4 (top, black line) shows the relation of the band gaps of alloyed $(ZnSe)_x(CuInSe_2)_{1-x}$ nanocrystals and compositions. It was found that alloying a tiny amount of $CuInSe_2$ into ZnSe will dramatically decrease the band gaps of alloyed $(ZnSe)_x(CuInSe_2)_{1-x}$ nanocrystals. In contrast, the band gaps of $CuInSe_2$-rich alloyed nanocrystals are not sensitive with the change of alloyed compositions. As shown in Figure S1, Supporting Information, the bowing parameter b is strongly dependent on the $CuInSe_2$ content. This result is consistent with those already reported for alloyed $(ZnS)_x$-$(CuInS_2)_{1-x}$ and $(ZnS)_x(Cu_2SnS_3)_{1-x}$ nanocrystals.[15,17] Note that only alloying 15% $CuInSe_2$ into ZnSe the band gap of alloyed nanocrystals will cover the whole visible light region, thus providing the possibility of synthesis of nontoxic quantum dots emitting in the UV−vis−NIR region.

Figure 5 on the right shows UV−vis−NIR absorption spectra of $CuInSe_xS_{2-x}$ nanocrystals. The calculated optical band gaps of $CuInS_2$ and $CuInSe_2$ nanocrystals are 1.43 and 0.98 eV, respectively, which are slightly lower than those of the corresponding bulk materials (1.53 and 1.02 eV).[40] The alloyed $CuInSe_xS_{2-x}$ nanocrystals displayed tunable band gaps in the range from 1.43 to 0.98 eV, further confirming formation of homogeneous alloys. In contrast to alloyed $(ZnSe)_x(CuInSe_2)_{1-x}$ nanocrystals, alloyed

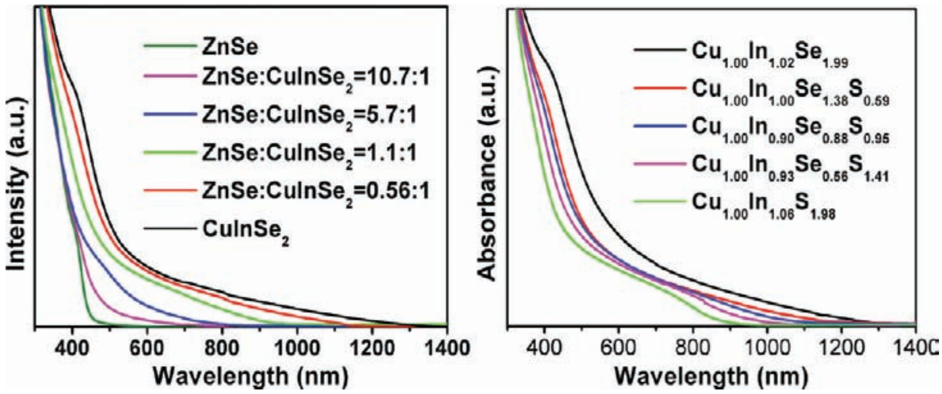

Figure 5. UV−vis−NIR absorption spectra of alloyed $(ZnSe)_x(CuInSe_2)_{1-x}$ and $CuInSe_xS_{1-x}$ nanocrystals.

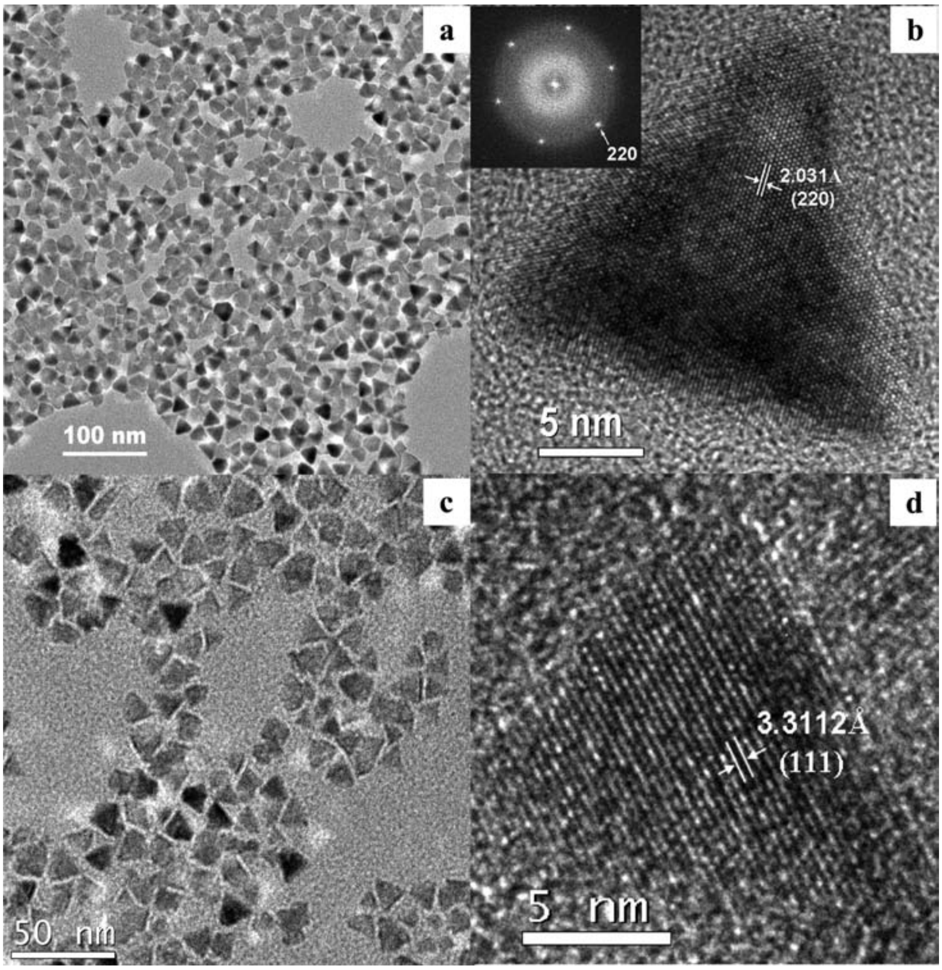

Figure 6. (a) TEM image of $(ZnSe)_{0.5}(CuInSe_2)_{0.5}$ nanocrystals. (b) HR-TEM image of a $(ZnSe)_{0.5}(CuInSe_2)_{0.5}$ nanocrystal and its FFT (inset). (c) TEM image of $CuInSe_{1.0}S_{1.0}$ nanocrystals. (d) HR-TEM image of a $CuInSe_{1.0}S_{1.0}$ nanocrystal.

$CuInSe_xS_{2-x}$ nanocrystals exhibit a linear relationship between the band gap and the composition (Figure 4, bottom).

Figure 6a and 6c show transmission electron microscopy (TEM) images for alloyed $(ZnSe)_{0.5}(CuInSe_2)_{0.5}$ and $CuInSe_{1.0}S_{1.0}$ nanocrystals. They both exhibit a narrow size distribution and have an average size of 17.1 and 15.0 nm, respectively, which are very close to the sizes calculated from their XRD patterns by the Scherrer equation. High-resolution TEM (HR-TEM) images (Figure 6b and 6d) clearly indicate that these nanoparticles are single crystalline and triangular in shape. A fast Fourier transform (FFT) (inset of Figure 6b) was used to measure the average spacing of the (220) plane for zinc blende $(ZnSe)_{0.5}(CuInSe_2)_{0.5}$ nanocrystal, and it was found to be 2.031 Å. For pure $CuInSe_2$ and ZnSe nanocrystals, their TEM images are shown in Figure S2, Supporting Information.

The chemical compositions of alloyed $(ZnSe)_x(CuInSe_2)_{1-x}$ nanocrystals were studied by energy-disperse X-ray spectroscopy

dx.doi.org/10.1021/ic201083r |Inorg. Chem. 2011, 50, 11958–11964

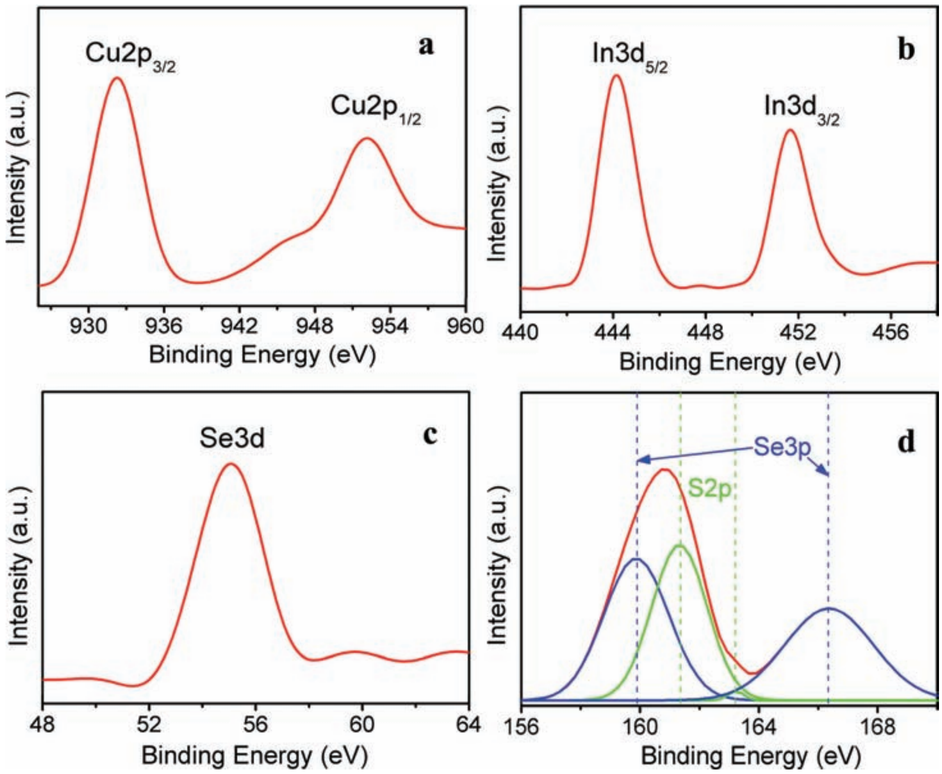

Figure 7. XPS spectra of alloyed $CuInSe_xS_{2-x}$ nanocrystals: (a) Cu2p, (b) In3d, (c) Se3d, and (d) S2p and Se3p.

(EDS) (Figure S3, Supporting Information). Compositions of the alloyed nanocrystals can be readily controlled by changing the ratio between the precursors (see Table S1, Supporting Information). X-ray photoelectron spectroscopy (XPS) (Figure S4, Supporting Information) was also applied to determine the chemical composition of $(ZnSe)_{0.5}(CuInSe_2)_{0.5}$ nanocrystals. XPS spectra of $(ZnSe)_{0.5}(CuInSe_2)_{0.5}$ nanocrystals confirmed the presence of the following elements: copper (Cu2p at 931.3 and 951.2 eV), zinc (Zn2p at 1021.4 and 1044.3 eV), indium (In3d at 443.8 and 451.4 eV), and selenium (Se3d at 54.1 eV).

In addition, the chemical compositions and valence states of alloyed $CuInSe_xS_{2-x}$ nanocrystals were also investigated by means of EDS (Figure S5, Supporting Information) and XPS (Figure 7). The ratios of Se-to-S in alloyed $CuInSe_xS_{2-x}$ nanocrystals are well consistent with those of the selenium and sulfur precursors (Table S2, Supporting Information). In Figure 7, the Cu 2p core splits into 2p3/2 (932.2 eV) and 2p1/2 (952.1 eV) peaks and In 3d shows two peaks at 444.1 and 451.6 eV. The observed binding energy values of Cu 2p and In 3d are in good accordance with those reported in the literature for the $CuInS_2$ nanocrystals,[9,37] suggesting that the valence states of Cu and In are +1 and +3. Se 3d shows a peak at 55.1 eV, and the two peaks located at 161.3 and 163.2 eV were assigned to S 2p with a valence of −2.

3. CONCLUSION

In summary, metastable zinc blende $CuInSe_2$ nanocrystals were synthesized by a hot-injection approach, which enables formation of alloyed $(ZnSe)_x(CuInSe_2)_{1-x}$ and $CuInSe_xS_{2-x}$ nanocrystals with a monophase zinc blende structure over the entire composition range. The disparities of the crystal structure and precursor reactivity between $CuInSe_2$ and ZnSe as well as $CuInSe_2$ and $CuInS_2$ vanished. The band gaps of alloyed $(ZnSe)_x$-$(CuInSe_2)_{1-x}$ and $CuInSe_xS_{2-x}$ nanocrystals can be tuned in the range from 2.82 to 0.96 eV and 1.43 to 0.98 eV, which covers the optimal band gap of 1.3 eV for single-junction solar cell applications. These alloyed nanocrystals with a broad tunable band gap have a high potential for photovoltaic and photocatalytic applications. Furthermore, it is quite possible to synthesize homogeneous alloyed $(ZnSe)_x(CuInSe_2)_{1-x}$/ZnS core/shell quantum dots emitting in the UV−vis−NIR region for replacement of highly toxic cadmium- and mercury-based quantum dots such as CdS, CdSe, CdTe, HgTe, etc.

4. EXPERIMENTAL SECTION

I. Chemicals. CuCl, $ZnCl_2$, $InCl_3 \cdot 4H_2O$, sulfur powder (99.999%), selenium powder (99.9%), and oleylamine (OM, 80−90%) were purchased from Aladdin Inc. Oleic acid (90%) was obtained from Aldrich. All chemicals were used as received.

II. Synthesis of $(ZnSe)_x(CuInSe_2)_{1-x}$ Nanocrystals. First, 0.474 g of (6.0 mmol) selenium was dissolved in 60 mL of oleylamine at 200 °C for 3 h. In a typical synthesis of $(ZnSe)_{0.5}(CuInSe_2)_{0.5}$ nanocrystals, 8.0 mL of Se/oleylamine solution (∼0.8 mmol) was added to a 50 mL three-neck flask and the reaction mixture was heated to 130 °C. The inside of the flask was degassed by a vacuum pump for 10 min, and argon gas was charged from the balloon. This procedure was repeated three times to remove the oxygen and water. Then, the temperature was increased to 300 °C. A 1.0 mL amount of oleylamine solution containing equal molar amounts (0.1 mmol each) of $ZnCl_2$, CuCl, and $InCl_3$ was heated to 220 °C on a hot plate and then swiftly injected into the flask under magnetic stirring. After 5 min, the crude solution was cooled to room temperature. The poorly capped nanocrystals were centrifuged first for 4 min at 4000 rpm. Then the nanocrystal solution was precipitated with 20 mL of ethanol. The purified nanocrystals were redispersed in toluene for UV−vis−NIR, TEM, and XRD measurements. The same procedure as above was employed to synthesize other alloyed $(ZnSe)_x(CuInSe_2)_{1-x}$ nanocrystals.

III. Synthesis of $CuInSe_xS_{2-x}$ Nanocrystals. The Cu/In stock solutions were prepared by dissolving 2.0 mmol of CuCl and 2.0 mmol of $InCl_3 \cdot 4H_2O$ in 20 mL of oleylamine at 180 °C for 30 min. Then, this stock solution was stored in an electric oven at 70 °C until use.

In a typical synthesis of $CuInSe_{1.0}S_{1.0}$ nanocrystals, 12.8 mg (0.4 mmol) of sulfur, 31.6 mg (0.4 mmol) of selenium, 0.3 mL of oleic acid, and 8.0 mL of oleylamine were loaded to a 50 mL three-neck flask and the reaction mixture was heated to 130 °C. Oxygen and water were removed by the procedure mentioned above. Subsequently, the temperature was elevated to 240 °C. A 1.0 mL amount of Cu/In stock solution in a small vial was heated to 180 °C on a hot plate and then swiftly injected into the flask under magnetic stirring. After 5 min, the crude solution was cooled to 180 °C and then precipitated with 30 mL of ethanol and further isolated by centrifugation and decantation. The same procedure as above was applied to synthesize other alloyed $CuInSe_xS_{2-x}$ nanocrystals. The yields of alloyed $(ZnSe)_x(CuInSe_2)_{1-x}$ and $CuInSe_xS_{2-x}$ nanocrystals after purification were about 80−90%.

IV. Characterization. The powder XRD patterns were recorded using a Bruker D8 FOCUS X-ray diffractometer. The simulated XRD patterns of $CuInSe_2$ were obtained using Diamond 3.0. The lattice mismatch was calculated via the following function: $\delta = 2|(a_2 - a_1)|/(a_2 + a_1) \times 100\%$, where a is the a-axis lattice constant. UV−vis−NIR absorption spectra were measured by a Shimadzu UV-3600, and the optical band gap (E_g) was obtained by extrapolating the linear portion of the absorption spectrum to $h\nu$ axis. TEM images were taken on a FEI Tecnai G2 F20 with an accelerating voltage of 200 kV. Energy-disperse spectroscopy (EDS) spectra were obtained using a scanning electron microscope (Hitachi S-4800) equipped with a Bruker AXS XFlash detector 4010. X-ray photoelectron spectra (XPS) were measured with VG ESCALAB MK (VG Co., U.K.) at room temperature by using a Mg Kα X-ray source ($h\nu$ = 1253.6 eV) at 14 kV and 20 mA. The binding energy was calibrated by the C1s (284.6 eV).

ASSOCIATED CONTENT

Supporting Information. EDS spectra, chemical compositions, additional TEM images, and XPS spectra of alloyed $(ZnSe)_x(CuInSe_2)_{1-x}$ nanocrystals. This material is available free of charge via the Internet at http://pubs.acs.org.

AUTHOR INFORMATION

Corresponding Author
*E-mail: pan@ciac.jl.cn (D.P.); hongjie@ciac.jl.cn (H.Z.); morphology@163.com (X.H.).

Author Contributions
The first two authors contributed equally to this work.

ACKNOWLEDGMENT

This work was partially supported by a startup fund from Changchun Institute of Applied Chemistry, the National Natural Science Foundation of China (Grant No. 21071142; 51172229), the Fund for Creative Research Groups (Grant No. 20921002), and the Natural Science Foundation for Young Scientists of Jilin Province (20100105).

REFERENCES

(1) Zhong, X.; Feng, Y.; Knoll, W.; Han, M. *J. Am. Chem. Soc.* **2003**, *125*, 13559.
(2) Zhong, X.; Han, M.; Dong, Z.; White, T.; Knoll, W. *J. Am. Chem. Soc.* **2003**, *125*, 8589.
(3) Deng, Z.; Yan, H.; Liu, Y. *J. Am. Chem. Soc.* **2009**, *131*, 17744.
(4) Bailey, R. E.; Nie, S. *J. Am. Chem. Soc.* **2003**, *125*, 7100.
(5) Sunc, C.; Gardner, J. S.; Long, G.; Bajracharya, C.; Thurber, A.; Punnoose, A.; Rodriguez, R. G.; Pak, J. J. *Chem. Mater.* **2010**, *22*, 2699.
(6) Pan, D. C.; Wang, X. L.; Zhou, Z. H.; Chen, W.; Xu, C. L.; Lu, Y. F. *Chem. Mater.* **2009**, *21*, 2489.
(7) Tang, J.; Hinds, S.; Kelley, S. O.; Sargent, E. H. *Chem. Mater.* **2008**, *20*, 6906.
(8) Panthani, M. G.; Akhavan, V.; Goodfellow, B.; Schmidtke, J. P.; Dunn, L.; Dodabalapur, A.; Barbara, P. F.; Korgel, B. A. *J. Am. Chem. Soc.* **2008**, *130*, 16770.
(9) Chiang, M.; Chang, S.; Chen, C.; Yuan, F.; Tuan, H. *J. Phys. Chem. C* **2011**, *115*, ASAP article.
(10) Colvin, V. L.; Schlamp, M. C.; Alivisatos, A. P. *Nature* **1994**, *370*, 354.
(11) Coe, S.; Woo, W. K.; Bawendi, M.; Bulovic, V. *Nature* **2002**, *420*, 800.
(12) Stolt, L.; Hedstrom, J.; Kessler, J.; Ruckh, M.; Velthaus, K. O.; Schock, H. W. *Appl. Phys. Lett.* **1993**, *62*, 597.
(13) AbuShama, J.; Johnston, S.; Moriarty, T.; Teeter, G.; Ramanathan, K.; Noufi, R. *Prog. Photovoltaics Res. Appl.* **2004**, *12*, 39.
(14) Guo, Q.; Ford, G. M.; Hillhouse, H. W.; Agrawal, R. *Nano Lett.* **2009**, *9*, 3060.
(15) Pan, D. C.; Weng, D.; Wang, X. L.; Xiao, Q. F.; Chen, W.; Xu, C. L.; Yang, Z. Z.; Lu, Y. F. *Chem. Commun.* **2009**, *28*, 4221.
(16) Wang, X.; Pan, D.; Weng, D.; Low, C.; Rice, L.; Han, J.; Lu, Y. *J. Phys. Chem. C* **2010**, *114*, 17293.
(17) Liu, Q.; Zhao, Z.; Lin, Y.; Guo, P.; Li, S.; Pan, D.; Ji, X. *Chem. Commun.* **2011**, *47*, 964.
(18) Dai, P.; Shen, X.; Lin, Z.; Feng, Z.; Xu, H.; Zhan, J. *Chem. Commun.* **2010**, *46*, 5749.
(19) Torimoto, T.; Adachi, T.; Okazaki, K. I.; Sakuraoka, M.; Shibayama, T.; Ohtani, B.; Kudo, A.; Kuwabata, S. *J. Am. Chem. Soc.* **2007**, *129*, 12388.
(20) Tsuji, I.; Kato, H.; Kudo, A. *Chem. Mater.* **2006**, *18*, 1969.
(21) Gremenoka, V. F.; Zaretskaya, E. P.; Siarheyeva, V. M.; Bente, K.; Schmitz, W.; Zalesski, V. B.; Moller, H. J. *Thin Solid Films* **2005**, *487*, 193.
(22) Bodnar, I. V.; Gremenok, V. F.; Schmitz, W.; Bente, K.; Doering, T. *Cryst. Res. Technol.* **2004**, *39*, 301.
(23) Lee, W.; Do, Y. *Bull. Korean Chem. Soc.* **1995**, *16*, 588.
(24) Gan, J. N.; Tauc., J.; Lambrecht, V. G; Robbins, J. M. *Phys. Rev. B* **1975**, *12*, 5797.
(25) Wagner, G.; Lehmanna, S.; Schorr, S.; Spemann, D.; Doering, T. *J. Solid State Chem.* **2005**, *178*, 3631.
(26) Allen, P. M.; Bawendi, M. G. *J. Am. Chem. Soc.* **2008**, *130*, 9240.
(27) Nose, K.; Omata, T.; Otsuka-Yao-Matsuo, S. *J. Phys. Chem. C* **2009**, *113*, 3455.
(28) Guo, Q.; Kim, S. J.; Kar, M.; Shafarman, W. N.; Birkmire, R. W.; Stach, E. A.; Agrawal, R.; Hillhouse, H. W. *Nano Lett.* **2008**, *8*, 2982.
(29) Ramanathan, K.; Contreras, M. A.; Perkins, C. L.; Asher, S.; Hasoon, F. S.; Keane, J.; Young, D.; Romero, M.; Metzger, W.; Noufi, R.; Ward, J.; Duda, A. *Prog. Photovoltaics Res. Appl.* **2003**, *11*, 225.
(30) Vos, A. D. *J. Phys. D: Appl. Phys.* **1980**, *13*, 839.
(31) Scheer, R.; Walter, T.; Schock, H. W.; Fearheiley, M. L.; Lewerenz, H. *J. Appl. Phys. Lett.* **1993**, *63*, 3294.
(32) Contreras, M. A.; Egaas, B.; Ramanathan, K.; Hiltner, J.; Swartslander, A.; Hasoon, F.; Noufi, R. *Prog. Photovoltaics: Res. Appl.* **1999**, *7*, 311.
(33) Haug, F. J.; Rudmann, D.; Zogg, H.; Tiwari, A. N. *Thin Solid Films* **2003**, *431*−*432*, 431.
(34) Contreras, M. A.; AbuShama, J.; Hasoon, F.; Young, D. L.; Egaas, B.; Noufi, R. *Prog. Photovoltaics Res. Appl.* **2005**, *13*, 209.
(35) Liu, W.; Mitzi, D. B.; Yuan, M.; Kellock, A. J.; Chey, S. J.; Gunawan, O. *Chem. Mater.* **2010**, *22*, 1010.
(36) Hou, W.; Bob, B.; Li, S. H.; Yang, Y. *Thin Solid Films* **2009**, *517*, 6853.

(37) Pan, D.; An, L.; Sun, Z.; Hou, W.; Yang, Y.; Yang, Z.; Lu, Y. *J. Am. Chem. Soc.* **2008**, *130*, 5620.
(38) Norako, M. E.; Brutchey, R. L. *Chem. Mater.* **2010**, *22*, 1613.
(39) Wang, J.; Wang, Y.; Cao, F.; Guo, Y.; Wan, L. *J. Am. Chem. Soc.* **2010**, *132*, 12218.
(40) Neff, H.; Lange, P.; Fearheiley, M. L.; Bachmann, K. J. *Appl. Phys. Lett.* **1985**, *47*, 1089.